J Therm Anal Calorim (2012) 110:847–855
DOI 10.1007/s10973-011-1852-7

Comparison of rhodamine B degradation under UV irradiation by two phases of titania nano-photocatalyst

Mphilisi M. Mahlambi · Ajay K. Mishra · Shivani B. Mishra · Rui W. Krause · Bhekie B. Mamba · Ashok M. Raichur

Received: 21 June 2011 / Accepted: 3 August 2011 / Published online: 19 August 2011

Abstract Titania (TiO_2) nano-photocatalysts, with different phases, prepared using a modified sol–gel process were employed in the degradation of rhodamine at 10 mg L^{-1} concentration. The degradation efficiency of these nano-photocatalysts was compared to that of commercial Degussa P25 titania. It was found that the nanocatalysts calcined at 450 °C and the Degussa P25 titania had similar photoreactivity profiles. The commercial Degussa P25 nanocatalysts had an overall high apparent rate constant of (K_{app}) of 0.023 min^{-1}. The other nanocatalyst had the following rate constants: 0.017, 0.0089, 0.003 and 0.0024 min^{-1} for 450, 500, 550 and 600 °C calcined catalysts, respectively. This could be attributed to the phase of the titania as the anatase phase is highly photoactive than the other phases. Furthermore, characterisation by differential scanning calorimetry showed the transformation of titania from amorphous to anatase and finally to rutile phase. SEM and TEM characterisations were used to study the surface morphology and internal structure of the nanoparticles. BET results show that as the temperature of calcinations was raised, the surface area reduced marginally. X-ray diffraction was used to confirm the different phases of titania. This study has led to a conclusion that the anatase phase of the titania is the most photoactive nanocatalyst. It also had the highest apparent rate constant of 0.017 min^{-1}, which is similar to that of the commercial titania.

Keywords Nanocatalyst · TiO_2 photocatalyst · UV photodegradation · Rhodamine B (Rh B)

M. M. Mahlambi · A. K. Mishra (✉) · S. B. Mishra · R. W. Krause · B. B. Mamba
Department of Chemical Technology, University of Johannesburg, P.O. Box 17011, Doornfontein 2028, South Africa
e-mail: amishra@uj.ac.za

A. M. Raichur
Department of Materials Engineering, Indian Institute of Science, Bangalore 560012, India

Introduction

The use of nanocatalysts (especially titanium dioxide or titania or TiO_2) has gained wide recognition since they have the potential to tackle the 'difficult-to-remove' contaminants and thus are expected to play an important role in solving many serious environmental and pollution problems. In addition, the conventional water treatment methods fail to adequately deal with water quality problems hence aggravating the scarcity of potable water. This has resulted in the need for the development of new and/or improved cost-effective technologies that can effectively address the challenges of providing sufficient water of an acceptable quality.

The provision of clean water by municipalities and water-governing bodies is essential for human health and in South Africa the demand is fast exceeding the supply [1]. The effects of global warming, effluents from domestic, agricultural and industrial works as well as the failure of the conventional water treatment methods to adequately deal with water quality problems have aggravated the scarcity of potable water [1]. This has resulted in the need for the development of new and/or improved cost-effective technologies that can effectively address the challenges of water quality. The use of nanocatalysts (especially titanium dioxide or TiO_2) has gained wide recognition since they have the potential to tackle the 'difficult-to-remove' contaminants like chlorinated phenols and industrial dyes and

are thus expected to play an important role in solving many serious environmental and water pollution problems [2].

Titanium dioxide (TiO_2 or titania) is a metal oxide semiconductor that has been extensively studied as a photocatalyst. As a photocatalyst titania has been used in coating self-cleaning surfaces, environmental purifiers and antifogging mirrors [3]. TiO_2 has gained more prominence than most semiconductors because of its properties which include, amongst others, long-term stability, non-toxicity, low price and superior photo-reactivity [4–13]. This photocatalytic activity is dependent on various parameters like crystallinity, impurities, surface area and density of surface reactive sites; however, the most important factor is crystallinity [13–16]. The photocatalytic reactions are initiated when the TiO_2 semiconductor absorbs energy (a photon or hv) and an electron is excited from the valence band to the conduction band, a gradual second order transition [17]. This happens if the energy of the photon is equal to or exceeds the band gap ($E_g = 3.0$–3.2 eV) [18, 19]. The electron (e^-) and the hole (h^+) act as the redox pair, and if these charges do not combine, they are prone to oxidation and reduction, respectively [12, 19]. The separated two charge carriers (e^- and h^+) drive the photo-electrochemical oxidation–reduction reactions with the redox molecules at the semiconductor surface [20].

In addition, because of these redox properties, titania has been used for the degradation of various toxic organic pollutants; the photocatalyst 'attacks' pollutants and converts them into benign compounds (e.g., water and CO_2), it also converts heavy metal ions (in solution) into less toxic ones and water photosplitting into H_2 and O_2 [5, 20]. Generally, it is widely accepted that the anatase phase of the titania is more reactive than the rutile phase and this enhanced photoreactivity is attributed to the higher Fermi level (by approximately 0.1 eV) of the anatase compared to that of the rutile phase [17, 21]. This therefore means that the synthesis of a controlled phase composition is essential for highly photocatalytically active nanocatalysts. However, a combined phase titania phase has not been extensively studied. Most articles report exclusively either on anatase or rutile titania phases, none report on the comparison on the photoactivity between two phases or more so a combined titania phase.

Recent studies on the applications of TiO_2 include, amongst others, its use as imprinted binary oxides, e.g., SiO_2–TiO_2 to photocatalytically degrade 2,4-dichlorophenol [12] or TiO_2–Fe_2O_3 to enhance the thermal behaviour of haematite ceramic systems [22] as well as an in situ coating of MWCNTs with sol–gel TiO_2 nanoparticles to enhance its visible light sensitivity [23]. Moreover, TiO_2 has been used to coat cellulosic fabric to enhance flame-retardancy in the synthesis of a new framework of products known as intelligent textiles [24]. Also, the semi-conductor thermochromic properties of TiO_2 have been exploited and used to study the semiconductor-to-metal phase transitions at a critical temperature, T_c [17]. This is useful in the synthesis of commercial window coating with TiO_2 thin films [17]. The presence of HOMO and LUMO energy levels in TiO_2 semiconductors helps in the fabrication of solar cells based on organic semiconductors since these cells can absorb a photon and convert it into electrical energy [25]. And finally, due to the extraordinary high dielectric constant of titanium compounds, titanium products have a promising role for capacitor applications, microelectronic devices, microwaves and mobile phones since it makes it possible to miniaturize passive microwave devices [26].

This study is therefore aimed at the comparison on the photodegradation activity of these titania phases on an industrial dye [Rhodamine B (Rh B)]. Also, a study on a mixed phase (calcined at 500 and 550 °C, which had less and much rutile phases of the titania, respectively) was studied. Rh B was chosen because it is one of the major pollutants obtained from textile and photographic industry effluents [27]. It is part of the xanthene group dyes and has achieved its prominent use due to its good stability as a laser material hence its photodegradation is important with regards to textile effluents. Also, photodegradation kinetics has been studied to understand the nature of the degradation mechanism of the dye. The photocatalytic reactions are initiated when the TiO_2 semiconductor absorbs energy (a photon or hv) and an electron is excited from the valence band to the conduction band. This happens if the energy of the photon is equal to or exceeds the band gap ($E_g = 3.0$–3.2 eV) [18, 19]. This therefore means that the correct phase composition is essential for the synthesis of highly photocatalytically active nanocatalysts that can overcome the chances of electron–hole recombination and thermal instability.

Experimental

Materials and methods

Titanium (IV) tetraisopropoxide (TTIP) (99%) was obtained from Sigma-Aldrich (Germany) and used without further purification. Formic acid (98%) was purchased at Merck and AR grade *n*-propanol was sourced from SD's Fine Chem (Pty) Ltd., and was distilled before usage.

Synthesis of the nanocrystalline photocatalysts

For the synthesis of the anatase-rich titania nanocatalysts, TTIP was hydrolysed through an esterification reaction between formic acid and propanol [28]. TTIP (10 mL,

0.334 mol) was dissolved in propanol (48 mL, 0.642 mol) and the reaction mixture was stirred for 20 min. Formic acid (13 mL, 0.535 mol) was gradually added whilst stirring gently. After stirring the reaction mixture for about 20 min, a white precipitate (titanium hydroxide) was gradually formed. This mixture was then stirred for further 2 h period, aged at room temperature for another 2 h and filtered. The filtered residue was then repeatedly washed with copious amounts of propanol and Millipore water; thereafter it was dried overnight in an oven at 80 °C. It was then ground into fine powder in a mortar and pestle and then calcined at 450, 500, 550 and 600 °C to obtain nanosized TiO_2 photocatalysts. All experiments were carried out at room temperature.

Characterization of the nanocatalysts

TG/DTA analysis

A METZSCH STA 409 PC/PG instrument was used to study the thermal properties of the synthesized nanogels. The TG part of the instrument measures the heat stability (mass loss) of the nanoparticles whilst the DTA accounts for the transformations that the nanoparticles undergo as a function of temperature. Samples were calcined in a muffle furnace. Heating was done under nitrogen with a flow rate of 20 mL min^{-1} and the heating rate was 10 °C min^{-1} at a temperature range of 25 and 1000 °C.

X-ray diffraction (XRD) measurements

The different phases of TiO_2 were determined using powder XRD. The XRD measurements were carried out using an X'Pert Pro MPD PANalytical powder diffractometer operating in the reflection mode with Cu-Kα radiation. The XRD chromatograms were recorded over an angular range of 10–90 °C (2θ) and with a step size of 0.02° and a collection time of 0.3 s ($\lambda = 0.154060$ nm). A shape factor K is used in XRD and crystallography to correlate the size of sub-micrometre particles, or crystallites. The Debye–Scherrer equation, $D = K\lambda/B\cos\theta$, was used to correlate the particle size, where the constant $K = 0.89$, $\lambda = 0.154060$ nm is the X-ray wavelength, B is the full width half maximum (FWHM) of the catalyst, and θ is the diffracting angle. The JCPDS XRD library software was used to confirm the Miller planes of the titania nanoparticles.

BET surface area analysis

To study the surface area of the synthesized nanoparticles, a Smart Sorb 92/93, which is an automated gas adsorption analyzer, was used. The samples were degassed at 100 °C under nitrogen flow for 90 min before the determination of their surface area. Surface area is believed to be an important parameter when studying the catalytic efficiency of the nanocatalysts since a high surface area means more active sites for extensive catalysis.

TEM, SEM and EDX spectroscopy

The spectroscopic measurements of the synthesized nanoparticles were studied using a JEOL J2100 F TEM, and a FEI-SIRION SEM to analyse and visualise the quality and morphology of the synthesized catalysts, respectively. The SEM was coupled with an EDX detector and this was used to determine the chemical composition of the nanoparticles.

Evaluation of photocatalytic activity

The photocatalytic activity of these TiO_2 nanophotocatalysts was studied using 100 mL (10 mg L^{-1}) Rh B. The red dye was poured into a beaker and placed in an UV photoreactor which was set inside a 1 m × 70 cm-wooden box. The solution was stirred using a magnetic stirrer for 30 min before irradiation with the UV light (dark, i.e., control experiment). This was done to establish an adsorption–desorption equilibrium between the dye and the catalyst surface. The UV irradiation lamp was about 10 cm away from the reactant solution and aliquots of 2 mL were extracted from the reaction chamber at 30 min interval to study the extent of the degradation. To establish the amount of Rh B degraded by the titania photocatalysts, an UV/Vis spectrophotometer (T60U Spectrophotometer, PG Instruments Ltd., UK) was used (Fig. 1).

The UV photoreactor used throughout this study had a jacketed quartz beaker with dimensions of 3.4 cm inner diameter, 4 cm outer diameter and 21 cm length. A high-pressure 125 W mercury vapour lamp (Samson, India) was used as the UV irradiation source. The suspended titania nanoparticles [100 mg, 5 mg L^{-1} dye (100 mL)] were

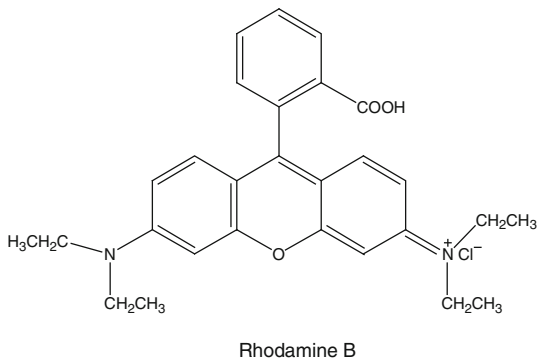

Fig. 1 Structure of Rh B

used to study the photoreactivity of the nanoparticles. The entire photoreactor setup was enclosed in a wooden box (1 m × 70 cm).

Results and discussions

Thermal analysis of titania nanoparticles

Figure 2 shows the differential scanning calorimetry (DSC) and TG thermograms whilst Fig. 3 shows the derivative curves of the thermograms. The TG thermogram can be divided into two stages. In the first stage, i.e., from 100 to 300 °C there is a constant mass loss of about 16%. This is due to dehydration and removal of organic residues (*n*-propanol) from the titania gel [22]. There is a further 4% mass loss between 300 and 400 °C which is associated with the transformation of the titania from the amorphous to the anatase phase (i.e., the combustion of TiOH to form TiO_2 nanoparticles) [28]. From above 400 °C up to 1000 °C there was no further mass loss. This is confirmed by the derivative curve in Fig. 3, which shows a negative peak at about 100 °C, another negative peak at 220 °C, and a constant straight line between 400 and 1000 °C.

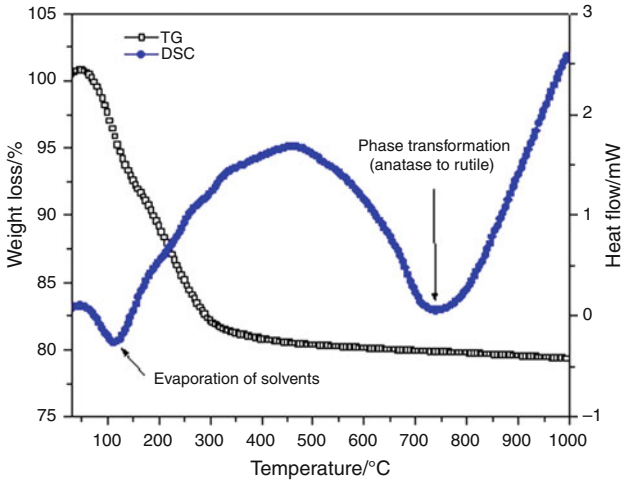

Fig. 2 TGA and DSC thermograms of titania nanoparticles

The DSC thermogram also exhibits similar peaks, i.e., two stages. It shows an endothermic peak at about 100 °C and another endothermic peak at about 682 °C (Fig. 2). However, to fully understand the transformation that the titania undergoes, a derivative curve of the DSC thermogram was studied (Fig. 3). From the derivative curve, four distinct peaks were observed. The first two were observed at about 100 °C (dehydration and removal of organic residues) and at about 216 °C (phase transformation from amorphous to anatase phase) [28]. The other two peaks were observed at about 290 °C (combustion of chelating esters) and finally at about 682 °C which is associated with the transformation of the titania from the anatase to the rutile phase [22, 29]. Both the anatase and rutile titania phases usually grow from TiO_6 through the rearrangement of the octahedral shape. It is widely accepted that the rearrangement of the phase through the edge sharing favours the formation of the rutile phase (i.e., above 520 °C) whilst the anatase phase is favoured by rearrangement through the face sharing below 520 °C [28, 30]. These observations are further explained by the XRD data.

XRD characterization

The XRD patterns obtained at different calcination temperatures are shown in Fig. 4. The amorphous phase (gels dried at 80 °C) show broad peaks which indicate less crystallinity. The XRD peaks obtained at calcination temperatures of 450 and 500 °C corresponds to the tetragonal anatase titania phase of the JCPDS CAS No. 21-1272

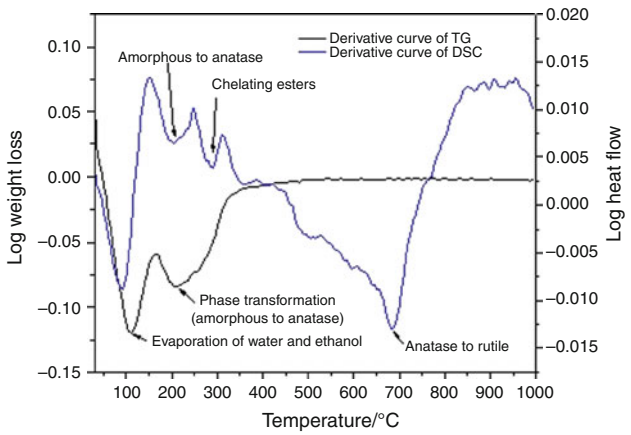

Fig. 3 Derivative curves of the DSC and TGA thermograms

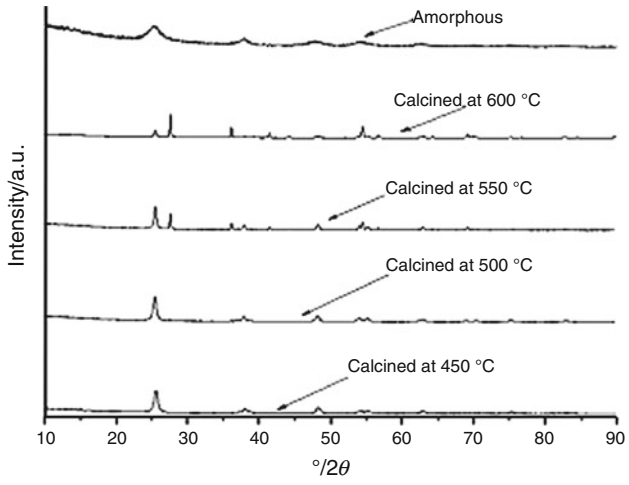

Fig. 4 XRD patterns of the titania calcined at different temperatures

(JCPDS catalogue). The peaks that were observed at $2\theta = 25.21$ (101), 37.53 (004), 47.87 (200), 53.53 (106) and $2\theta = 62.37$ (215) indicate the successful synthesis of the anatase phase of TiO_2. Of note is the absence of the peaks $2\theta = 27.5$ (a rutile-phase peak) due to the (110) reflection and $2\theta = 30.8$ (121) which is a brookite phase, and this is an indication of the absence of these phases in our synthesized titania [31].

However, as the calcination temperature was increased to above 500 °C, the rutile phase developed ($2\theta = 27.5$) and became more pronounced at 600 °C. At 550 °C an almost equal amount of the anatase and rutile phase is observed. These results are consistent with the DSC and TGA results obtained and further confirm that as the temperature is raised to above 520 °C, the rearrangement of the phase through the edge sharing favours the formation of the rutile phase [22, 29, 30].

The average crystal size of the TiO_2 nanoparticles was estimated using FWHM (B in the Debye–Scherrer equation, $D = K\lambda/B\cos\theta$), and were found to increase with increasing temperature. For the amorphous phase the crystal size was found to be 8.63 nm. As the calcination temperature was increased particle sizes of 22.63, 23.35, 35.43 and 49.80 nm were recorded for the titania calcined at 450, 500, 550 and 600 °C, respectively. This therefore indicates that as the calcination temperature is increased, the crystal size of the nanoparticles also increases.

BET surface area analysis

The effect of the calcination temperature on the surface area of the nanoparticles was also studied and it was found to decrease with an increase in calcination temperatures. The decrease in the surface area was expected as the increase in crystal size should result in the decrease in surface area. The results of the BET surface area analysis are shown in Table 1 and they indicate that the calcination temperature is inversely proportional to the surface area. It is well known that the amorphous phase of the titania has a large surface area; however, it has a low photoreactivity because of surface defects [32]. It was therefore no surprise that the amorphous titania exhibited a large surface area which decreased with an increase in calcination temperatures.

Table 1 BET surface area, band gap and particle size analysis of the TiO_2 nanoparticles

Nanoparticle	Surface area/ $m^2\ g^{-1}$	Band gap/ eV	Particle size/nm
Amorphous titania	281.5	–	8.63
TiO_2 calcined at 450 °C	86.83	3.18	22.63
TiO_2 calcined at 500 °C	52.5	3.19	23.35
TiO_2 calcined at 550 °C	22.72	3.16	35.43
TiO_2 calcined at 600 °C	7.78	3.10	49.8

SEM, TEM and EDX analysis

The SEM micrographs shown in Fig. 5 indicate that the TiO_2 nanoparticles synthesized were relatively spherical in shape. Although, the nanoparticles appear agglomerated, the agglomeration is irrespective of the calcination temperatures. The TEM images (Fig. 6) were also studied to further study the nanoparticles. From the TEM images, it can be seen that the nanoparticles are also agglomerated, disordered yet still spherical (Fig. 6b). From the corresponding electron diffraction (ED) patterns (a) and (b), it can be observed that the rings (a) suggest a nanocrystalline form of the anatase titania phase (101) whilst the disordered pattern (b) is characteristic of the rutile phase (110).

The EDX pattern (Fig. 7) was used to determine the elemental composition of the synthesized titania and it gave evidence of the presence of Ti^{4+} and O^{2-} ions that make up the titania matrix [33]. It further showed the absence of impurities in the titania crystal, providing evidence of the successful synthesis of pure titania nanoparticles.

UV–Vis analysis—band gap studies

The UV–Vis spectrophotometry was used to determine the band gap (E_g) of the titania nanoparticles (Table 1). The equation, $E_g = h(c/\lambda)$, was used where E_g is the band gap, h is the Planck's constant, c is the speed of light ($m\ s^{-1}$) and λ is the wavelength (nm). A tangent of the plot of $h\nu$ versus $(\alpha h\nu)^2$ gives an estimate of the band gap where α is the absorbance and ν is the wave number. Figure 8 shows the plot of $h\nu$ versus $(\alpha h\nu)^2$, and the extrapolated tangent indicates an estimate E_g, i.e., band gap.

The indirect method (from UV–Vis spectrophotometry) for the determination of the band gap was used and its plot is shown in Fig. 7. The band gap for the titania calcined at 450 °C was found to be 3.18 eV which is comparable to the value of 3.2 eV reported in the literature for the anatase phase [31, 34, 35]. The band gaps of the TiO_2 nanoparticles calcined at 500, 550 and 600 °C were found to be 3.19, 3.16 and 3.10 eV, respectively (Table 1). This decrease in band gap is expected because the rutile phase is reported to have a smaller band gap than the anatase phase [35]. Therefore, as the calcination temperature is increased, more anatase titania is converted to rutile, hence the decrease in band gap.

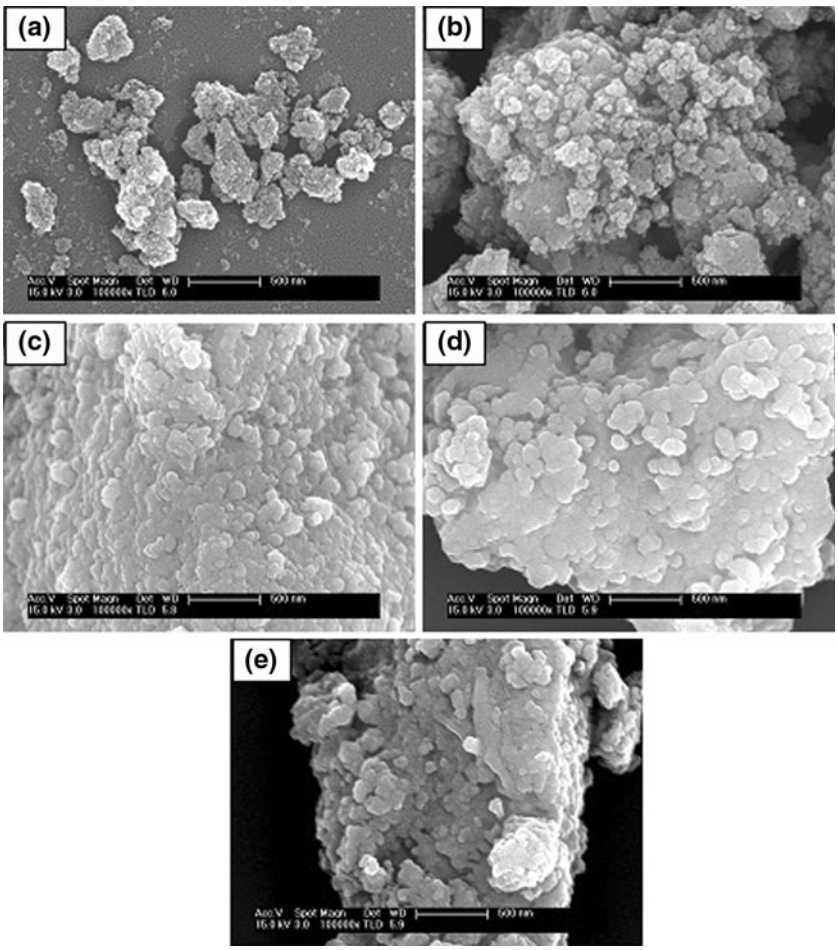

Fig. 5 SEM micrographs of the titania calcined at different temperatures: **a** amorphous, **b** 450, **c** 500, **d** 550 and **e** 600 °C

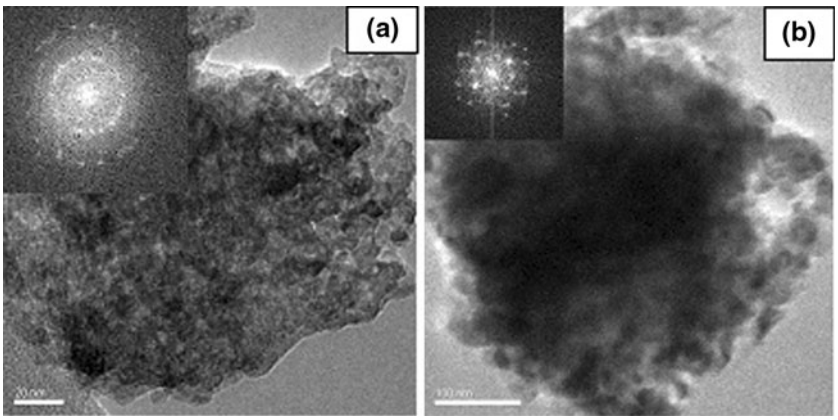

Fig. 6 TEM micrographs of titania calcined at **a** 450 and **b** 600 °C

Degradation studies

The degradation of Rh B by the synthesized nanocrystalline titania nanoparticles under UV light was studied for the commercial (Degussa P25), 450, 500, 550 and 600 °C calcined titania nanocatalysts. The results obtained are presented in Fig. 9. For the photocatalytic degradation experiments, 10.0 mg L^{-1} (ppm) Rh B and 100 mg L^{-1} TiO_2 concentrations were used. These were done in a photoreactor chamber at room temperature. As a control experiment, the dye was exposed to UV irradiation for 5 h without the catalysts to establish whether any degradation had occurred and it was observed that there was no degradation in the absence of titania nanoparticles. These experiments were done using titania nanoparticles in the form of a suspension and the reaction mixture was stirred constantly; 2 mL aliquots of Rh B was taken at 30 min interval and analyzed the amount of Rh B degraded.

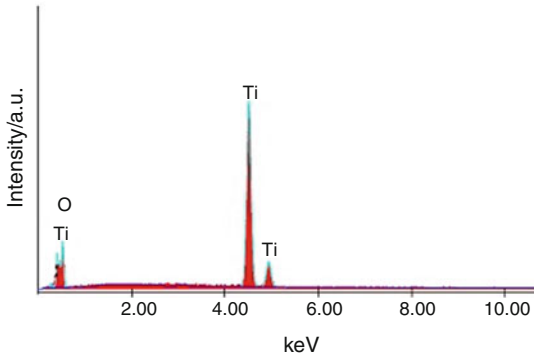

Fig. 7 EDX pattern of titania nanoparticles

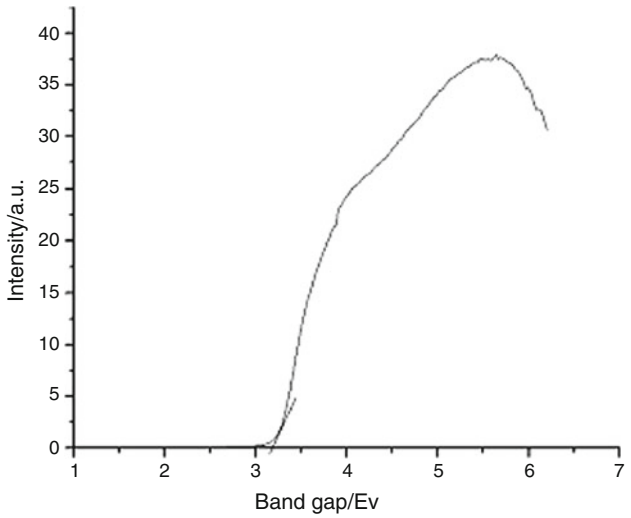

Fig. 8 Band gap estimation of the synthesized TiO_2 nanoparticles (calcined at 450 °C)

From these analyses it was observed that the commercial, i.e., Degussa P25 titania had degraded about 54% of the dye within the first 30 min itself (Fig. 9). The titania nanocatalysts calcined at 450 °C had degraded 59%, whilst the titania calcined at 500, 550 and 600 °C had the slowest degradation of Rh B at 9.5, 2.4 and 1.4%, respectively, within the first 30 min. The 450 °C calcined titania show a high degradation rate than even the commercial Degussa P25 titania within the first 30 min of degradation. This however decreases as the degradation time is increased. A general trend observed is that the Degussa P25 had the fastest degradation rate (it completely degraded the dye within 180 min) followed by the titania calcined at 450 °C (270 min) and finally the titania calcined at 600 °C (510 min) (Table 2).

Reaction kinetics

From the results obtained, the Degussa P25 showed the highest reaction rate. This is confirmed by the linear

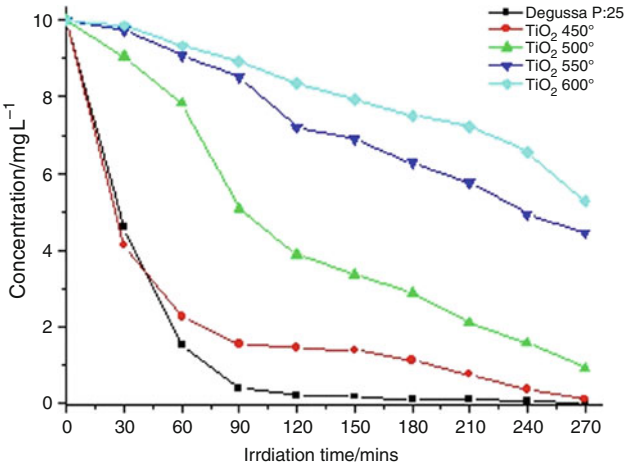

Fig. 9 Graph showing degradation of Rh B by titania nanoparticles (average of 3 experimental counts)

Table 2 Summary of the degradation of Rh B with respect to time

TiO_2 nanoparticle	% Rh B degraded after 30 min	Time taken for complete Rh B degradation/min
Degussa P25	54	180
Calcined at 450 °C	59	270
Calcined at 500 °C	9.5	360
Calcined at 550 °C	2.4	420
Calcined at 600 °C	1.4	510

transform of the TiO_2 degradation graphs (Fig. 10). It had an apparent rate constant (K_{app}) of 0.023 min^{-1}. The other nanocatalyst had the following rate constants: 0.017, 0.0089, 0.003 and 0.0024 min^{-1} for 450, 500, 550 and 600 °C calcined catalysts, respectively. The apparent rate constant was chosen as the basic kinetic parameter for the photocatalysts because it allows for the determination of photocatalytic activity independent of the previous adsorption period in the dark and the concentration of the Rh B remaining in the solution [18]. The apparent first order kinetic equation $\ln(C_0/C) = K_{app}t$ was used to fit the experimental data. K_{app} is apparent rate constant, C is the solution phase concentration and C_0 is the concentration at $t = 0$ [36].

The slow degradation rate shown by the titania synthesized in our laboratory could be due to synthetic defects, especially because some agglomeration of particles was evident (SEM images), hence less surface area was available resulting in fewer reaction sites for the degradation to take place. Also, the titania calcined from between 500 and 600 °C was less photoactive than the titania calcined at 450 °C. This could be due to the fact that as the calcination temperature is increased, there is an increase in the particle size (Table 1) hence a decrease in the surface area resulting

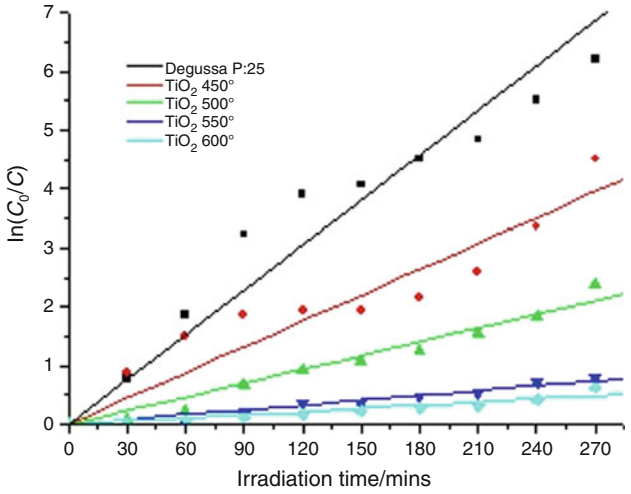

Fig. 10 Linear transform $\ln(C_0/C) = f(t)$ of the kinetic curves of the degradation of Rh B by the different nanocatalysts (average of 3 experimental counts)

in a decrease in the photocatalytic activity of the nanoparticles.

Conclusions

The crystalline titania nanoparticles, which were successfully synthesized using a modified sol–gel technique, were found to effectively degrade 10 mg L^{-1} concentration of Rh B. The anatase phase of the titania had the highest photoactivity and this photoactivity was found to decrease as the content of the rutile phase increased. This was further confirmed by the apparent rate constants which were found to have the following rate constants: 0.017, 0.0089, 0.003 and 0.0024 min^{-1} for 450, 500, 550 and 600 °C calcined catalysts, respectively.

The degradation studies showed that the commercial titania (Degussa P25) had the fastest degradation rate followed by the titania calcined at 450, 500, 550 and 600 °C had the slowest degradation rates. This is attributed to the fact that as the calcination temperature is increased, there is an increase in the particle size resulting in a decrease in the surface area, hence a decrease in the photocatalytic activity of the nanoparticles. This can be as a result of the decrease in the photocatalytic sites as the crystallite particles increase in size due to rutilation on heating. We therefore propose that by optimizing the synthesis conditions of the anatase phase of the titania nanoparticles enhanced photoreactivity would be achieved.

Acknowledgements The authors are grateful to the University of Johannesburg, DST/Mintek NIC for financial support and the Indian Institute of Science, Bangalore, India for providing the infrastructure to carry out most of this research study.

References

1. Shutte CF, Focke W. Evaluation of nanotechnology for application in water and waste water treatment and related aspects in South Africa. WRC Report No. KV 195/07. 2007;1–24.
2. Chen X, Mao SS. Titanium dioxide: synthesis, properties, modifications, and applications. Chem Rev. 2007;107:56–2891.
3. Ananpattarachi J, Kajitvichyanukul P, Seraphin S. Visible light absorption ability and photocatalysis oxidation activity of various interstitial N-doped TiO_2 prepared from different nitrogen dopants. J Hazard Mater. 2009;168:253–61.
4. Tungudomwongsa H, Leckie J, Mill T. Photocatalytic oxidation of emerging contaminants: kinetics and pathways for photocatalytic oxidation of pharmaceutical compounds. J Adv Oxid Technol. 2006;9:59–64.
5. Ahn W-Y, Sheeley SA, Rajh T, Cropek DC. Photocatalytic reduction of 4-nitrophenol with arginine-modified titanium dioxide nanoparticles. Appl Catal B. 2007;74:103–10.
6. Yu JG, Yu HG, Cheng B, Zhao XJ, Yu JC, Ho WK. The effect of calcinations temperature on the surface microstructure and photocatalytic activity of TiO_2 thin films prepared by liquid phase deposition. J Phys Chem B. 2003;107:13871–9.
7. Zhao JC, Wu TX, Wu KQ, Oikawa K, Hidaka H, Serpone N. Photoassisted degradation of dye pollutants; degradation of the cationic dye rhodamine B in aqueous anionic surfactant/TiO_2 dispersions under visible light irradiation: evidence for the need of substrate adsorption on TiO_2 particles. Environ Sci Technol. 1988;32:2394–400.
8. Xu YM, Langford CH. UV–or visible-light-induced degradation of X3B on TiO_2 nanoparticles: the influence of adsorption. Langmuir. 2001;17:897–902.
9. Honda K, Fujishima A. Electrochemical photolysis of water at a semiconductor electrode. Nature. 1972;238:37–8.
10. Tada H, Yanamoto M, Ito S. Promoting effect of MgO_x submonolayer coverage of TiO_2 on the photoinduced oxidation of anionic surfactants. Langmuir. 1999;15:3699–702.
11. Fox MA, Dulay MT. Heterogeneous photocatalysis. Chem Rev. 1993;93:341–57.
12. Han D, Li Y, Jia W. Preparation and characterization of molecularly imprinted SiO_2–TiO_2 and photo-catalysis for 2,4-dichlorophenol. Adv Mater Lett. 2010;1(3):188–92.
13. Pulisova P, Bohacek J, Sburt J, Szatmary L, Bezdicka P, Vecernikova E, Balek V. Thermal behaviour of titanium dioxide nanoparticles prepared by precipitation from aqueous solutions. J Them Anal Calorim. 2010;101:607–13.
14. Arya SK, Vats T, Sharma SN, Singh K, Narula AK. Effect of mercaptopropionic acid as linker on structural, thermal and optical properties of TiO_2–CdSe nanocomposites. J Therm Anal Calorim. 2011. doi:10.1007/s1093-011-1687-2.
15. Fu W, Yang H, Li M, Yang N, Zou G. Anatase TiO_2 nanolayer coating on cobalt ferrite nanoparticles for magnetic photocatalyst. Mater Lett. 2005;59:3530–4.
16. Ao Y, Xu J, Fu D, Yuan IC. A simple method to prepare N-doped titania hollow spheres with high photocatalytic activity under visible light. J Phys Chem Solids. 2008;69:2660–4.
17. Kiri P, Hyett G, Binions R. Solid state thermochromic materials. Adv Mater Lett. 2010;1(2):86–105.
18. Hoffmann MR, Martin ST, Choi W, Bahnemann DW. Environmental applications of semiconductor photocatalysis. Chem Rev. 1995;95:69–96.
19. Hagen JP. Using lab-report grading rubrics with calibrated peer review. Abstr Am Chem Soc. 2003;225:U542–1542.
20. Bessekhoud Y, Robert D, Weber JV. Synthesis of photocatalytic TiO_2 nanoparticles: optimization of the preparation conditions. J Photochem Photobiol A. 2003;157:47–53.

21. Porkodi K, Arokiamary SD. Synthesis and spectroscopic characterization of nanostructured anatase titania: a photocatalyst. Mater Charact. 2007;58:495–503.
22. Moafi HM, Shojaie AF, Zanjanchi MA. Flame-retardancy and photocatalytic properties of cellulosic fabric coated by nano-sized titanium dioxide. J Therm Anal Calorim. 2011;104:717–24.
23. Chen L, Pang X, Yu G, Zhang J. In situ coating of MWNTs with sol–gel TiO_2 nanoparticles. Adv Mater Lett. 2010;1(1):75–8.
24. Sorescu M, Xu T. The effect of ball-milling on the thermal behaviour of anatase-doped haematite ceramic system. J Therm Anal Calorim. 2011;103:479–84.
25. Pode R. On the problem of circuit voltage in metal phthalocyanine/C60 organic solar cells. Adv Mater Lett. 2011;2(1):3–11.
26. Chamola A, Singh H, Naithani UC, Sharma S, Prabhat U, Devi P, Malik A, Srivastava A, Sharma RK. Structural, dielectric and electrical properties of lead zicronate titanate and $CaCu_3Ti_4O_{12}$ ceramic composite. Adv Mater Lett. 2011;2(1):26–31.
27. Murat A, Meltem A, Funda S, Nadir K, Ertugrul A, Hikmet S. A novel approach to the hydrothermal synthesis of anatase titania nanoparticles and the photocatalytic degradation of rhodamine B. Turk J Chem. 2006;30:333–43.
28. Zhu J, Zhang J, Chen F, Iino K, Anpo M. High activity TiO_2 photocatalysts prepared by a modified sol–gel method: characterization and their photocatalytic activity for the degradation of XRG and X-GL. Catalysis. 2005;35:261–8.
29. Kawahara T, Ozawa T, Iwasaki M, Tada H, Ito H. Photocatalytic activity of rutile-anatase coupled TiO_2 particles prepared by a dissolution–reprecipitation method. J Colloid Interface Sci. 2003; 267:377–81.
30. Dhage SR, Choube VD, Samuel V, Ravi V. Synthesis of nanocrystalline TiO_2 at 100 °C. Mater Lett. 2004;58:2310–3.
31. Lei Y, Zhang LD, Fan JC. Fabrication, characterization and Raman study of TiO_2 nanowire arrays prepared by anodic oxidative hydrolysis of $TiCl_3$. Chem Phys Lett. 2001;338:231–6.
32. Battacharyya A, Kawi S, Ray MB. Photocatalytic degradation of orange II by TiO_2 catalysts supported on adsorbents. Catal Today. 2004;98:431–9.
33. Jing D, Zhang Y, Guo L. Study on the synthesis of Ni doped mesoporous TiO_2 and its photocatalytic activity for hydrogen evolution in aqueous methanol solution. Chem Phys Lett. 2005;415:74–8.
34. Mogyorosi M, Dekany I, Fendler JH. Preparation and characterization of clay mineral intercalated titanium dioxide. Langmuir. 2003;19:2938–46.
35. Wang T, Wang H, Xu P, Zhao X, Liu Y, Chao S. The effect of properties of semiconductor oxide thin films on photocatalytic decomposition of dyeing waste water. Thin Solid Films. 1998;334: 103–8.
36. Matos J, Laine J, Hermann JM. Synergy effect in the photocatalytic degradation of phenol on a suspended mixture of titania and activated carbon. Appl Catal B. 1998;18:281–91.